Ceramics International 43 (2017) 12572–12578

Contents lists available at ScienceDirect

Ceramics International

journal homepage: www.elsevier.com/locate/ceramint

New optimized method for low-temperature hydrothermal production of porous ceramics using diatomaceous earth

Arianit A. Reka[a], Blagoj Pavlovski[b], Petre Makreski[c,*]

[a] Faculty of Natural Sciences and Mathematics, University of Tetovo, Ilinden n.n., 1200 Tetovo, Republic of Macedonia
[b] Faculty of Technology and Metallurgy, Ss. Cyril and Methodius University, Ruger Boskovic bb, 1000 Skopje, Republic of Macedonia
[c] Institute of Chemistry, Faculty of Natural Sciences and Mathematics, Ss. Cyril and Methodius University, Arhimedova 5, 1000 Skopje, Republic of Macedonia

ARTICLE INFO

Keywords:
Calcium silicate hydrate
Compressive strength
Diatomaceous earth
Hydrothermal synthesis
Porous ceramics

ABSTRACT

The aim of this study was to test the diatomaceous earth from a deposit near Rožden Village (Macedonia) as a raw material for low temperature hydrothermal production of porous ceramics. Hydrothermal synthesis of porous ceramics has been carried out under saturated steam pressure at 130 °C for a period of 1, 2 and 3 h. The objective of this work was to investigate the impact of slaked lime, autoclave curing time, autoclaving temperature and compaction pressure on the compressive strength and porosity of the products. During the hydrothermal synthesis, newly obtained calcium silicate hydrate dominates which give positive effect to the compressive strength and product porosity confirmed by X-ray powder diffraction. Moreover, a calcite was also evidenced by FTIR spectroscopy whose presence additionally increases the compressive strength of the hydrothermal products. The products obtained during the low-temperature hydrothermal reaction are classified as light porous ceramics with bulk density ranging from 0.71 to 0.91 g/cm^3 and compressive strength within 14.7–19.4 MPa.

1. Introduction

Production of porous ceramics with high porosity requires very careful approach. There are numerous methods for production of porous ceramic: use of filler grains with their own porosity; selection of a granular composition; use of additives producing pores on initial mixture; involvement of air into ceramics suspensions; blowing gas into a ceramic melt, etc.

The microstructure and properties of porous ceramics are controlled by the process by which they are prepared [1]. The properties of porous ceramics depend on the type of initial material, porosity and structure of the products. Structural and morphological characteristics of the obtained ceramics are porosity, pore size (and pore distribution by size), permeability and specific surface area. Porous ceramics have several main types of structure which depends on the pore formation method. The pore size can vary over a wide range from a fraction of a nanometer to a few millimeters [2,3].

Diatomaceous earth, as well as other inorganic materials that contain amorphous SiO_2 such as trepel, are convenient and promising materials for the production of porous ceramics due to its natural porosity, low density and mineralogical composition [4–8].

Hydrothermal production of ceramics offers many advantages over conventional ceramic production. The drying and firing process is replaced with a hydrothermal process, a process which occurs at much lower temperatures and takes shorter time that results with great energy savings. Hydrothermal technology can be used for the production of various types of ceramic materials form the special ceramics [9–15] and is also widely used for the production of conventional porous ceramic products [16–24].

Amorphous SiO_2 from the diatomaceous earth during the hydrothermal process with calcium hydroxide results in the formation of calcium silicate (C-S-H) gel as a product. The type of C-S-H phase has a huge impact on the porosity and the strength of the final product.

During the hydrothermal reaction of diatomaceous earth with calcium hydroxide, in addition to the C-S-H phase, various types of alkaline aluminocalcium-silicate-hydrate also occurs depending on the concentration of the alkaline, Ca, Al and Si [24,25].

Herein, we present new cheap, effective, low-cost and environmental friendly method using natural diatomaceous earth to fabricate light porous ceramic that can withhold large compressive strength. The product was further characterized by different physico-chemical techniques.

* Corresponding author.
E-mail address: petremak@pmf.ukim.mk (P. Makreski).

http://dx.doi.org/10.1016/j.ceramint.2017.06.132
Received 1 June 2017; Received in revised form 20 June 2017; Accepted 20 June 2017
Available online 21 June 2017

2. Material and methods

Diatomaceous earth from a deposit near Rožden Village (Republic of Macedonia) was used as starting raw material. Physical-mechanical analysis showed that diatomaceous earth represents white to gray rock with a massive homogeneous texture and shell-like fragility. The rock is light, soft, weakly bound, and in dry condition exhibit compressive strength of 3.5–4.5 MPa. The rock's bulk mass and porosity ranging from 0.55 to 0.60 g/cm^3 and 73–75%, respectively.

Various dry mixtures from diatomaceous earth and $Ca(OH)_2$ (Sigma-Aldrich) were prepared. The weight percentage of added calcium hydroxide varied from 3% to 28%. Water was added to the mixtures until 40% of moisture was reached including the calculated water content from $Ca(OH)_2$. Afterwards, the mixtures were placed in hermetically closed desiccator for 24 h to achieve distribution of even moisture level throughout the mixtures.

The samples were prepared to obtain cylindrical forms with diameter of 16 mm and height of 10 mm under pressure from 2 to 10 MPa. Subsequently, the samples were processed in autoclave for 1, 2 and 3 h at 130 °C and dried at 80 °C to constant mass. Subsequently, the samples were tested for compressive strength. Upon testing, the material was characterized by physical-mechanical methods and chemical analysis. The mineralogical composition was further analyzed by an X-ray powder diffraction (XRPD), thermal analysis (TGA/DTA), scanning electron microscopy (SEM) and transmission electron microscopy (TEM).

The diatomaceous earth was ball-milled for a period of 2.5 h. The results of the granulometric composition are obtained while performing wet sieve analysis and laser granulometric analysis.

XRPD analysis was performed on Rigaku Ultima IV X-ray diffractometer equipped with D/teX high-speed 1-dimensional detector using CuKα radiation (λ = 1.54056 Å) in 2θ range from 10 to 60°. The accelerating voltage and the current power were set to 40 kV and 40 mA, respectively.

DTA/TGA analyses of the diatomaceous earth were performed in air environment with *Stanton Redcroft* apparatus, under the following experimental conditions: temperature range from 20 to 1050 °C; speed of heating set to 10 °C/min; sample mass of 11.7 mg; and ceramic pot as a material carrier.

Scanning electron microscopy (SEM) of the products was performed with energy dispersive X-ray spectroscopy (EDX) employing FEI Quanta 3D FEG dual beam microscope.

The Perkin-Elmer FTIR system 2000 interferometer was employed to record the IR spectra in 4000–500 cm^{-1} range using the KBr pellet method. The spectral resolution was set to 4 cm^{-1} and the spectrum merged from 16 measurements.

Products were also analyzed by transmission electron microscopy (TEM) using Hitachi H-7650 apparatus (120 kV automatic microscope).

3. Results and discussion

3.1. Characterization of the raw material

3.1.1. Chemical analysis

The granulometric and chemical composition of the diatomaceous earth are given in Tables 1 and 2, respectively. The results revealed non time-consuming mechanical processing of the material because micron size was obtained after short milling time (Table 1). The chemical composition categorized the raw material as high quality diatomaceous earth suitable for potential production of various ceramic products (Table 2).

3.1.2. XRPD analysis

Results of the XRPD analysis of the diatomaceous earth (Fig. 1) depicts amorphous behavior of the sample manifested by the appearance of one complex “bump” widely positioned between 15 and 30° (2θ) with the maximum peaking in the 18–26.7° range. The region is characteristic for the strongest peaks in the debyegrams of all SiO_2 polymorphs modifications: quartz (26.674°), cristobalite (21.946°) and tridymite (21.638°). No additional peaks evolved confirming the amorphous character of the diatomaceous earth.

Table 1
Granulometric composition of diatomaceous earth obtained after ball milling for 2.5 h.

Size (μm)	Particle size distribution (%)
> 63	17.20
46–63	1.33
24–46	20.04
12–24	16.48
6–12	24.34
1–6	19.04
< 1	1.57

Table 2
Chemical composition of the diatomaceous earth.

Oxide	Mass (wt%)
SiO_2	92.62
Al_2O_3	1.41
Fe_2O_3	0.25
TiO_2	0.08
CaO	0.38
MgO	0.23
MnO	0.02
SO_3	0.07
P_2O_5	0.10
K_2O	0.29
Na_2O	0.10
LOI	4.23
Total	**99.78**

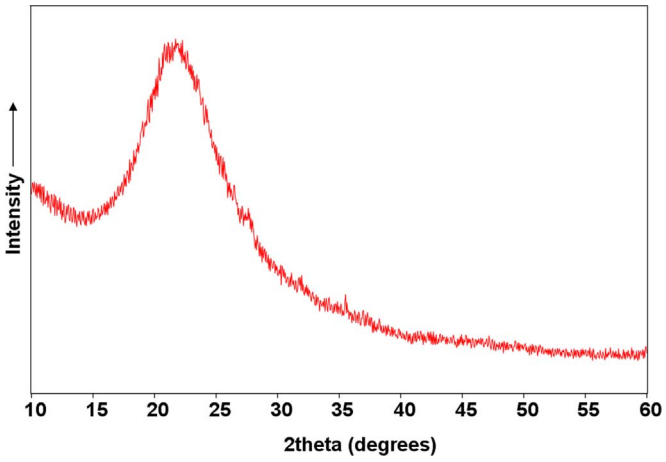

Fig. 1. XRPD analysis of the diatomaceous earth.

3.1.3. Thermal analyses

TGA/DTA results (Fig. 2) of the diatomaceous earth shows an intensive mass loss (7%) upon heating to the temperature of 250 °C explained by the elimination of the adsorbed water on the surface and on the pores of the diatomaceous earth. The maximum speed of the mass loss evidenced on the DTG curve occurs at 185 °C. The significantly decelerated mass loss is evidenced from 250 °C to 700 °C, whereas no further weight deficit occurred up to 1000 °C. The DTA curve depicts an exothermic peak at 940 °C that might be due to the crystallization of the amorphous phase (see 3.2.4).

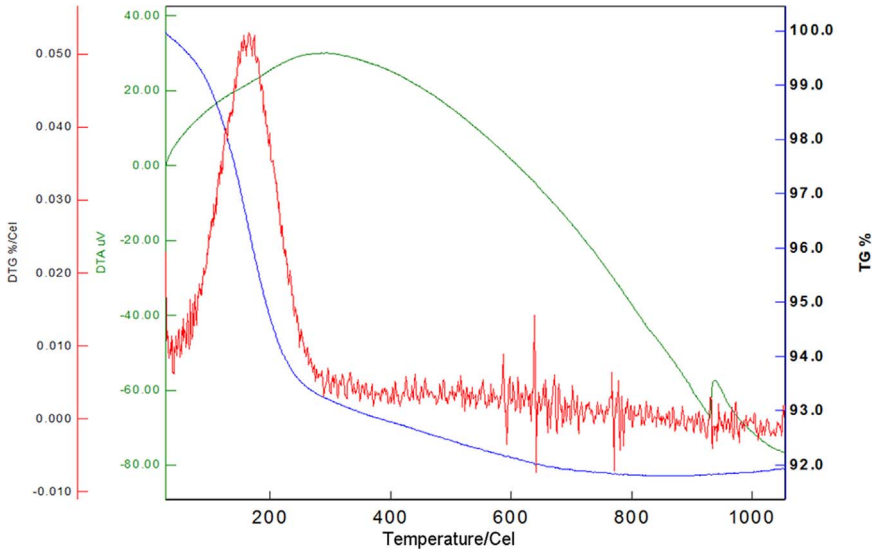

Fig. 2. DTA/TGA of the diatomaceous earth.

3.1.4. FTIR spectroscopy

The IR spectrum of the diatomaceous earth (Fig. 3) exhibits absorption bands at 793 cm^{-1} and 1048 cm^{-1} due to the presence of the amorphous SiO_2 in the sample, whereas the negligible absorption in the 3200–3700 cm^{-1} as well as the weak band at 1640 cm^{-1} appear from the stretching and bending vibrations from the adsorbed water. FTIR examinations of the diatomaceous earth provide valuable information for sample purity (no bands from impurities are registered) in accordance with the obtained results from the XRPD and chemical analysis.

3.1.5. SEM and TEM examinations

The results of the SEM analysis of the diatomaceous earth (Fig. 4) provide valuable information for the surface characteristics of this raw material, for the morphology (shape and size) as well as for its porosity (shape and size of the pores). Various skeletal forms are apparent on the SEM pictures of the diatomaceous earth particles (Fig. 4). Clearly visible nanometric pores on the surface make the analyzed diatomite very promising raw material for production of porous ceramics.

TEM examination (Fig. 5) closely resembles the results obtained from SEM measurements and revealed cylindrical shape and size of the diatomite's pores. The pores are open, not filled with powder material, peaking c.c. 1 μm in height and 0.3 μm in diameter.

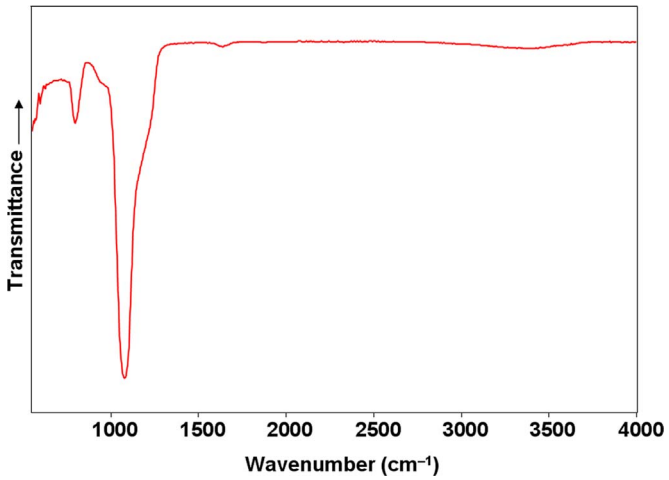

Fig. 3. IR spectrum of the diatomaceous earth.

3.2. Characterization of the obtained product

3.2.1. Physical-mechanical characteristics

The impact of autoclaving time on the compressive strength of the product (Fig. 6a) demonstrates increase of the product compressive strength as a function of the autoclaving time. The abrupt rise of the strength is monitored immediately after the second hour practically doubling its value until the beginning of the third hour. The autoclaving process was stopped because the hydrothermal product exhibited satisfying compressive strength much higher than 5 MPa.

In order to monitor the impact of the $Ca(OH)_2$ on the compressive strength of the autoclaved probes and to optimize the proposed method, mixtures with 3, 8, 13, 18, 23 and 28 wt% fractions of $Ca(OH)_2$ were prepared (Fig. 6b). The impact of $Ca(OH)_2$ content on the compressive strength of the samples compacted at 2 MPa and cured at 130 °C for 3 h rendered optimal results with 23 wt% $Ca(OH)_2$ showing product's maximum compressive strength of 14.7 MPa.

Procedure was further focused on preparation of samples with 23% of $Ca(OH)_2$ and 40% moisture at various pressures (2, 4, 6, 8 and 10 MPa) in order to determine the pressure for mixture formation relative to the compressive strength (Fig. 6c). Consequently, the samples were hydrothermally treated for a period of 3 h at 130 °C. After drying to constant mass at 80 °C, probes were tested for compressive strength and bulk density.

The impact of the compacting pressure on the bulk density of the products shows significant and linear increase of the bulk density up to 6 MPa (0.88 g/cm^3), whereas higher pressures have insignificant influence on the rise of the products' bulk density (Fig. 6d).

The physical-mechanical analyses were followed on the ceramic hydrothermal products (autoclaved for 3 h at 130 °C): bulk mass, specific mass, water absorption, porosity and determination of the compressive strength. The results from these investigation [23% $Ca(OH)_2$ at 2 MPa pressure of formation] are moved in Table 3.

3.2.2. XRPD characterization

The discussed wide peak observed in the diatomaceous earth (Fig. 1) appeared in non-autoclaved mixture of diatomaceous earth with 23 wt% $Ca(OH)_2$ (Fig. 7a) as well as in the corresponding hydrothermally treated product autoclaved in period of 3 h at 130 °C (Fig. 7b). In line with the expectations, the XRPD pattern of the non-autoclaved mixture resulted by the appearance of seven additional peaks that are attributed to the presence of $Ca(OH)_2$ phase (Fig. 7a). On the other hand, the XRPD of the hydrothermally treated sample resulted in absence of the $Ca(OH)_2$ peaks depicting the presence of the

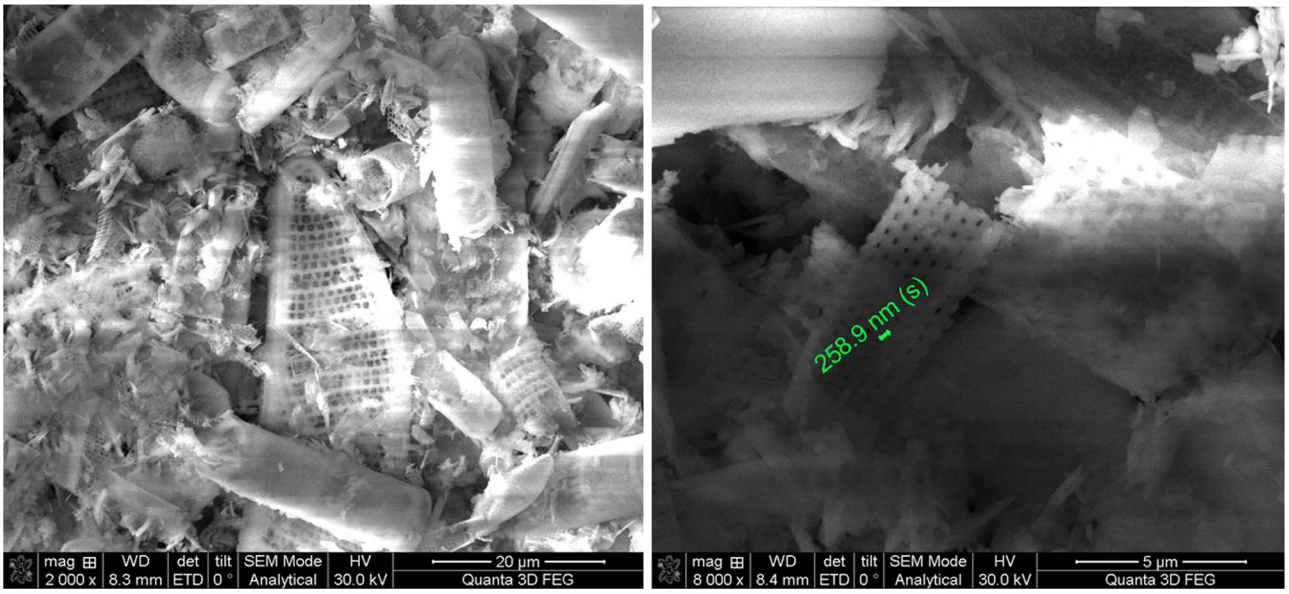

Fig. 4. SEM pictures of the diatomaceous earth.

newly formed phases (Fig. 7b). Namely, the evolved peaks strongly confirmed formation of calcium silicate hydrate (C-S-H) (I) as well as the presence of calcite, tobermorite and quartz. (C-S-H) (I) resembles poorly crystalline calcium silicate hydrate phase [26] whereas the amorphous hump centred around 20–25° indicates the presence of amorphous silica in addition to C-S-H (I). The asymmetry of the strongest peak is caused due to the integration of three different minerals with close *d*-values. The peak at 29.30° (2θ) is due to the presence of C-S-H (I) which overlaps the tobermorite peak at 28.89° (Fig. 7d) and calcite peak at 29.44° (Fig. 7e). Several weak intensity peaks also evolve from the mentioned phases as well from quartz (Fig. 7c). C-S-H (I) represents the dominant phase that highly influence on the compressive strength of the hydrothermally synthesized products.

3.2.3. FTIR spectroscopy

FTIR examinations of the hydrothermally treated probe (23 wt% $Ca(OH)_2$, T = 130 °C; t = 3 h) (Fig. 8a) shows additional bands, apart the bands evolving from the presence of unreacted diatomite. Their appearance is related to the products formed from the hydrothermal-induced reaction between diatomite and calcium hydroxide. Precisely, the bands at 877 cm^{-1} and 1423 cm^{-1} are prescribed to the calcite formation (Fig. 8a and b). The calcium silicate hydrate (C-S-H) formed during the hydrothermal treatment of the sample results in absorption band at 969 cm^{-1}. The presence of the bands at 790 cm^{-1}, 1104 cm^{-1} and 1645 cm^{-1} appear from the unreacted amorphous SiO_2 whereas the wide band in the region from 3600 to 3200 cm^{-1} and 1650 cm^{-1} band appear as result of bonded water in the amorphous SiO_2 and the bonded water in the newly formed C-S-H phase (Fig. 8a).

3.2.4. DTA/TGA examinations of products and further XRPD characterization

Thermal examinations of the hydrothermally treated probe (Fig. 9) shows mass loss integrated in three temperature intervals. The first temperature range extends to 215 °C resulting in 4.93% mass loss due to the separation of absorbed water from the surface and the open pores of the diatomite and the C-S-H. The second temperature interval occurs in 215–479 °C region and corresponds to smaller mass loss (2.69%). The mass loss during this temperature increase is ascribed to the combustion of the organic substance in diatomite. The most intensive loss in mass (12.5%) appears in the third temperature interval (479–694 °C) where separation of the water from the synthesized CSH takes place.

The exothermic peak occurring at the DT curve at 900 °C indicates the crystallization of amorphous SiO_2 into formation of wollastonite. The solid-solid transformation was confirmed by XRPD. Namely,

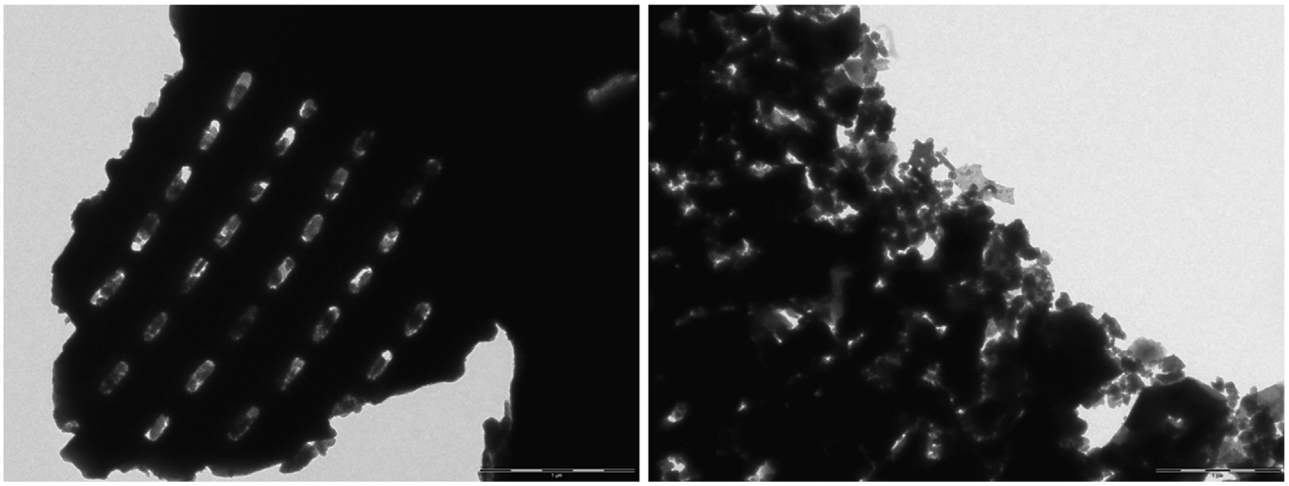

Fig. 5. TEM pictures of the diatomaceous earth.

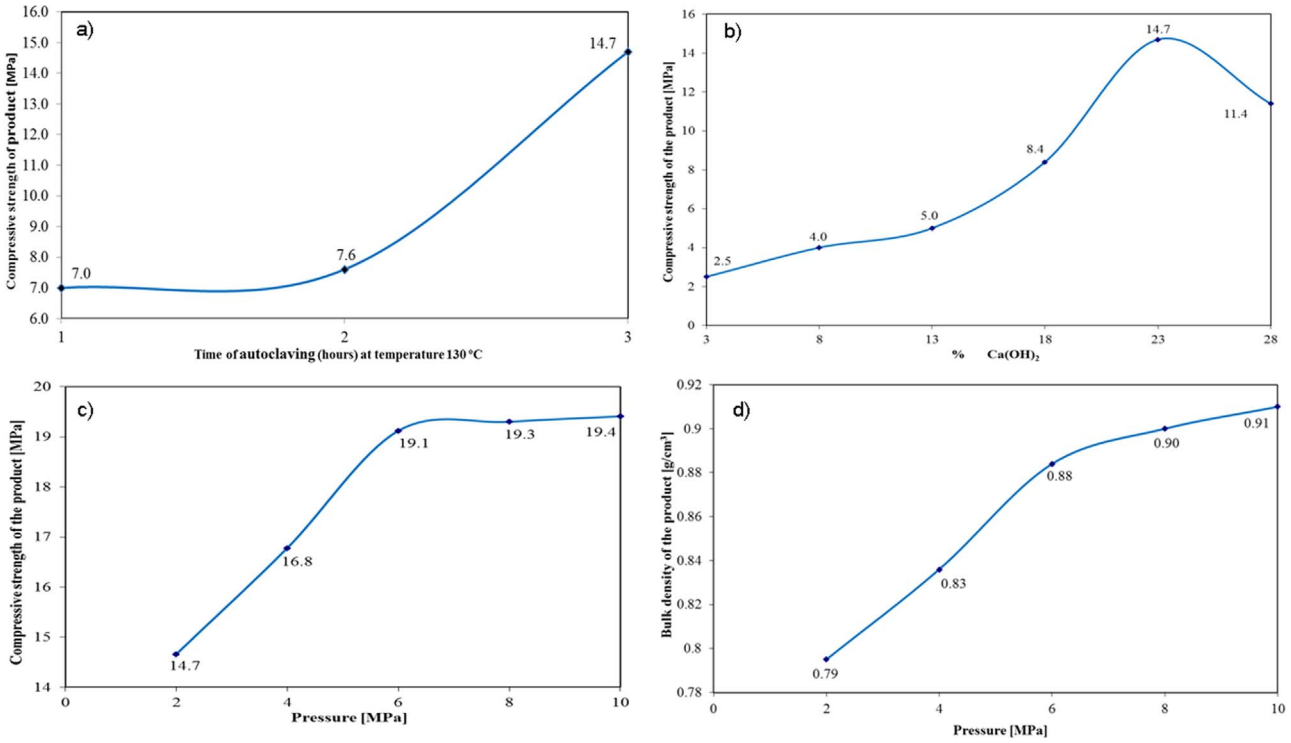

Fig. 6. The impact of autoclaving time (at T = 130 °C) on the compressive strength of the products (a). The influence of $Ca(OH)_2$ content on the compressive strength of the probes compacted at 2 MPa and cured at 130 °C for 3 h (b). Impact of the pressure on the compressive strength of the products (c). The impact of the compacting pressure on the bulk density of the products (d).

Table 3
Physical-mechanical properties of ceramic products.

Bulk density	0.79 g/cm^3
Specific mass	2.05 g/cm^3
Water absorption	52.63%
Open porosity	44.73%
Total porosity	58.53%

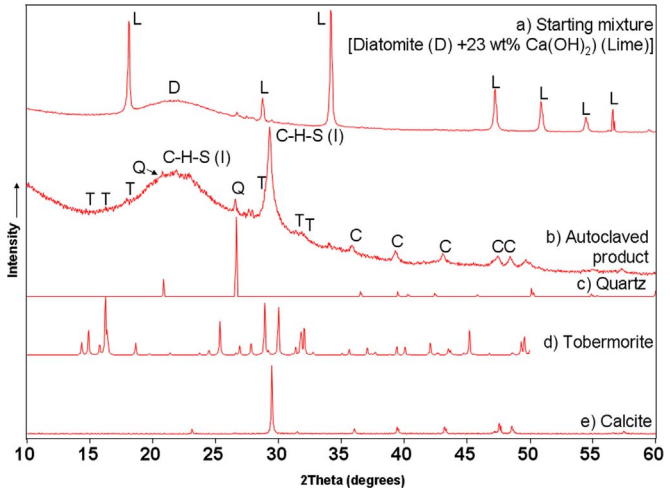

Fig. 7. XRPD diagrams of not-autoclaved mixture of diatomite with 23% $Ca(OH)_2$ (a) and the corresponding diagram of the autoclaved product (b), quartz (c), tobermorite (d) and calcite (e).

after completition of the TG run, the final product was subjected to structural analysis and the obtained XRPD pattern (Fig. 10a) showed great resemblance with the corresponding diagram of wollastonite, $CaSiO_3$ (Fig. 10b). The most characteristic peaks of wollastonite are marked by asterisks and appear at 2θ values: 11.53, 21.96, 23.16,

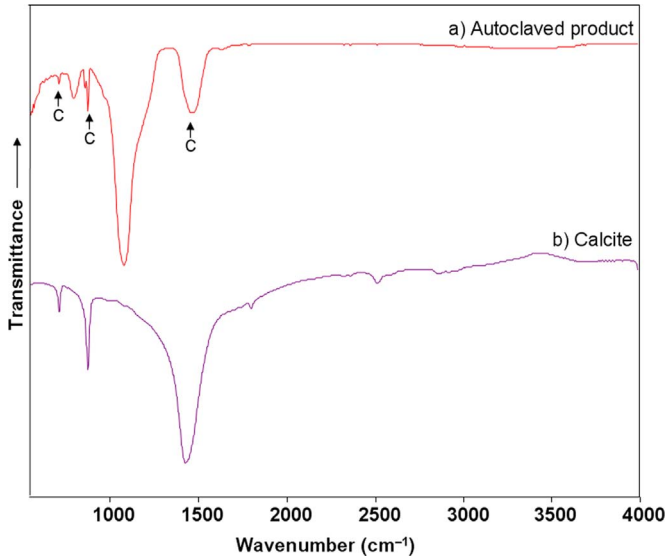

Fig. 8. FTIR spectrum of the hydrothermally treated probe with 23% $Ca(OH)_2$ autoclaved 3 h at 130 °C (a). The corresponding spectrum of calcite (b) is presented for comparison.

25.31, 26.91, 28.88, 29.98, 32.91, 35.05, 36.26, 38.32, 39.17, 41.29, 44.82, 49.76, 52.11, 53.31 and 57.42.

4. Conclusions

The examinations performed on this research showed that the diatomaceous earth from the deposit in Rožden (Macedonia) is very prominent material for the production of porous ceramic products under optimized method for low-temperature hydrothermal procedure. The results of the analysis showed best results for the mixture consisted of 23 wt% calcium hydroxide and 77 wt% diatomaceous earth, auto-

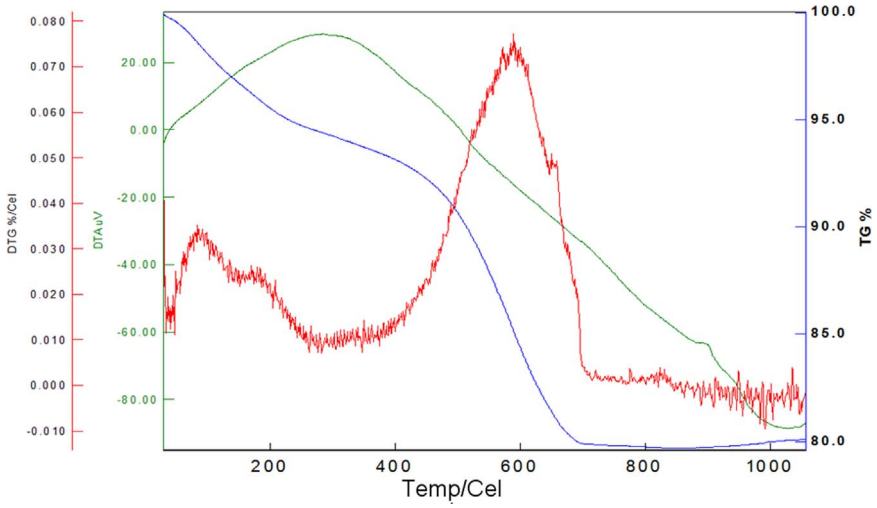

Fig. 9. TGA/DTA of probe with 23% $Ca(OH)_2$ hydrothermally treated for 3 h at 130 °C.

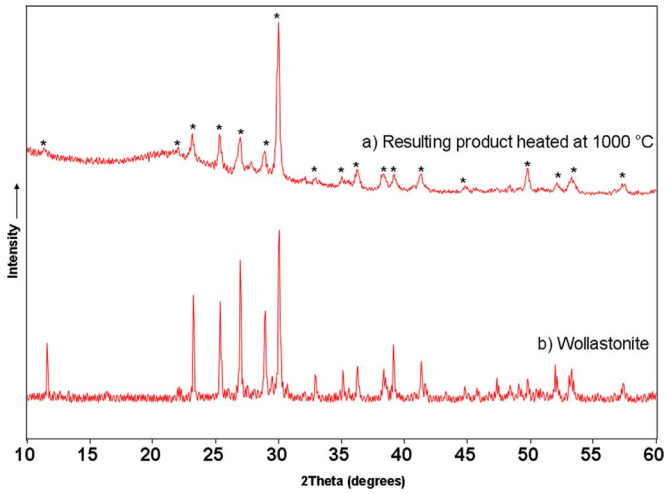

Fig. 10. XRPD confirmation that wollastonite was obtained as the resulting product was treated at 1000 °C (a). The corresponding diagram of wollastonite (b) is presented for comparison.

claved for 3 h at temperature of 130 °C. The product obtained under these conditions featured the following physical-mechanical properties: bulk density from 0.79 to 0.91 g/cm^3 specific mass 2.05 g/cm^3, water absorption 52.63%, open porosity 44.73%, total porosity 58.53%, and compressive strength 14.7–19.4 MPa. During the hydrothermal synthesis, the formation of calcium silicate hydrates was evidenced which has positive effect on the compressive strength and porosity of the products. The dominant formation of calcium silicate hydrates C-S-H (I) has the highest influence on the compressive strength of the hydrothermally obtained products. Besides the presence of the calcium silicate hydrates, small content of calcite was evidenced also having synergetic impact toward the compressive strength of the products.

The examinations showed that in addition to C-S-H, tobermorite enables expressed mechanical properties (compressive strength) of the low-temperature hydrothermal obtained product.

Acknowledgements

The authors thank the Ministry of Education and Science of Macedonia for providing financial support.

References

[1] Y.Q. Li, J.Q. Wu, Preparation, application, and development prospect of porous ceramics, Ceram. Eng. 12 (2000) 44–47.
[2] I. Ya Guzman, Certain principles of formation of porous ceramic structures. Properties and application (A review), Glass Ceram. 60 (2003) 280–283.
[3] M. Takahashi, M. Fuji, Synthesis and fabrication of inorganic porous materials: from nanometer to millimeter sizes, KONA Powder Part. J. 20 (2002) 84–97.
[4] A.A. Reka, T. Anovski, S. Bogoevski, B. Pavlovski, B. Boskovski, Physical-chemical and mineralogical-petrographic examinations of diatomite form deposit near village of Rozden, Republic of Macedonia, Geol. Maced. 28 (2014) 121–126.
[5] B. Cekova, B. Pavlovski, D. Spasev, A. Reka, Structural examinations of natural raw materials pumice and trepel from Republic of Macedonia, in: Proceedings of the XV Balkan Mineral Processing Congress, Sozopol, Bulgaria, 2013, pp. 73–75.
[6] B. Cekova, B. Pavlovski, V. Markoska, A. Reka, The adsorption character of zeolites, type 4a, obtained by natural raw trepel Bitola, R. Macedonia, Int. J. Eng. Sci. Innov. Technol. (IJESIT) 3 (2014) 449–454.
[7] A.A. Reka, B.H. Durmishi, A. Jashari, B. Pavlovski, N. Buxhaku, A. Durmishi, Physical-chemical and mineralogical-petrographic examinations of Trepel from Republic of Macedonia, Int. J. Innov. Stud. Sci. Eng. Technol. (IJESIT) 2 (2016) 13–17.
[8] B. Pavlovski, S. Jančev, L. Petreski, A. Reka, S. Bogoevski, B. Boškovski, Trepel – a peculiar sedimentary rock of biogenetic origin from the Suvodol village, Bitola, R. Macedonia, Geol. Maced. 25 (2011) 67–72.
[9] W.L. Suchanek, R.E. Riman, Hydrothermal synthesis of advanced ceramics powders, Adv. Sci. Technol. 45 (2016) 184–193.
[10] D. Losic, J.G. Mitchell, N.H. Voelcker, Diatomaceous lessons in nanotechnology and advanced materials, Adv. Mater. 21 (2009) 2947–2958.
[11] S. Murakami, K. Kato, Y. Enari, M. Kamitakahara, N. Watanabe, K. Ioku, Hydrothermal synthesis of porous hydroxyapatite ceramics composed of rod-shaped particles and evaluation of their fracture behaviour, Ceram. Int. 28 (2012) 1649–1654.
[12] J. Ortiz-Landeros, C. Gomez-Yanez, R. Lopez-Juarez, I. Davalos-Velasco, H. Pfeiffer, Synthesis of advanced ceramics by hydrothermal crystallization and modified related methods, J. Adv. Ceram. 1 (2012) 204–220.
[13] R.E. Riman, W.L. Suchanek, M.M. Lencka, Hydrothermal crystallization of ceramics, Ann. Chem. Sci. Mater. 27 (2002) 15–36.
[14] Y. Koseoglu, F. Alan, M. Tan, R. Yilgin, M. Ozturk, Low temperature hydrothermal analysis and characterization of Mn doped cobalt ferrite nanoparticles, Ceram. Int. 38 (2012) 3625–3634.
[15] K. Nakata, T. Kubo, C. Numako, T. Onoki, A. Nakahira, Synthesis and characterization of silicon-doped hydroxyapatite, Mater. Trans. 50 (2009) 1046–1049.
[16] F. Akhtar, Y. Rehman, L. Bergström, A study of the sintering of diatomaceous earth to produce porous ceramic monoliths with bimodal porosity and high strength, Powder Technol. 201 (2010) 253–257.
[17] Y. Jing, Z. Jing, E.H. Ishida, Relationship between porous and mechanical properties of hydrothermally synthesized porous materials from diatomaceous earth, Ind. Eng. Chem. Res. 52 (2013) 17865–17870.
[18] Y. Enriquez Mendez, M. Vlasova, I. Leon, M.G. Kakazey, M. Dominguez-Patino, L. Isaeva, T. Tomila, Low temperature synthesis of porous silicate ceramics, Sci. Sinter. 39 (2007) 39–49.
[19] H. Maeda, E.H. Ishida, Hydrothermal preparation of diatomaceous earth combined with calcium silicate hydrate gels, J. Hazard. Mater. 185 (2011) 858–861.
[20] Z. Matamoros-Veloza, J.C. Rendon-Angeles, K. Yanagisawa, M.M. Cisneros-Guerrero, M.A. Cisneros-Guerrero, Preparation of low-density porous glass-ceramics under hydrothermal hot pressing, in: Proceedings of the Joint 20th AIRAPT – 43rd EHPRG International Conference on High Pressure Science and Technology, 2005.
[21] Z. Jing, H. Maeda, K. Ioku, E.H. Ishida, Hydrothermal synthesis of mesoporous

materials from diatomaceous earth, Am. Inst. Chem. Eng. 53 (2007) 2114–2122.
[22] Z. Jing, S. Kato, H. Maeda, E.H. Ishida, Hydrothermal synthesis of mesoporous materials using diatomaceous earth, AIP Conf. Proc. 898 (2007) 193.
[23] H. Maeda, S. Kato, E.H. Ishida, Preparation of hydrothermal solidified mesoporous materials from diatomaceous earth for moisture control application, Int. J. Appl. Ceram. Technol. 6 (2009) 431–436.
[24] J. Chappuis, A new model for a better understanding of the cohesion of hardened hydraulic materials, Colloids Surf. A: Physicochem. Eng. 156 (1999) 223–241.
[25] J.M. Rivas Mercury, X. Turrillas, A.H. de Aza, P. Pena, Calcium aluminates hydration in the presence of amorphous SiO_2 at temperatures below 90 °C, J. Solid State Chem. 179 (2006) 2988–2997.
[26] G.M.N. Baston, A.P. Clacher, T.G. Heath, F.M.I. Hunter, V. Smith, S.W. Swanton, Calcium silicate hydrate (C-S-H) gel dissolution and pH buffering in a cementitious near field, Mineral. Mag. 76 (2012) 3045–3053.